

Accepted Manuscript

Constructing Stochastic Models for Dipole Fluctuations from Paleomagnetic Observations

Bruce Buffett, Abhijit Puranam

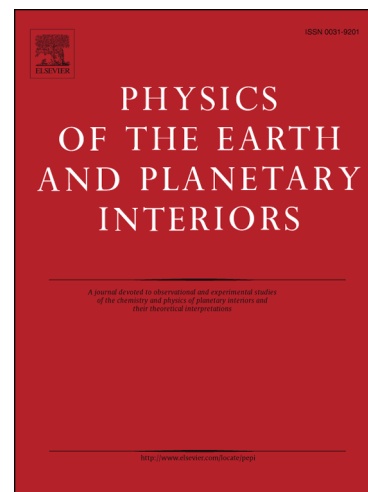
PII: S0031-9201(17)30114-0
DOI: <http://dx.doi.org/10.1016/j.pepi.2017.09.001>
Reference: PEPI 6080

To appear in: *Physics of the Earth and Planetary Interiors*

Received Date: 18 March 2017
Revised Date: 15 August 2017
Accepted Date: 1 September 2017

Please cite this article as: Buffett, B., Puranam, A., Constructing Stochastic Models for Dipole Fluctuations from Paleomagnetic Observations, *Physics of the Earth and Planetary Interiors* (2017), doi: <http://dx.doi.org/10.1016/j.pepi.2017.09.001>

This is a PDF file of an unedited manuscript that has been accepted for publication. As a service to our customers we are providing this early version of the manuscript. The manuscript will undergo copyediting, typesetting, and review of the resulting proof before it is published in its final form. Please note that during the production process errors may be discovered which could affect the content, and all legal disclaimers that apply to the journal pertain.



Constructing Stochastic Models for Dipole Fluctuations from Paleomagnetic Observations

Bruce Buffett^a, Abhijit Puranam^b

^a*Department of Earth and Planetary Science, University of California, Berkeley, CA 94720, USA (bbuffett@berkeley.edu)*

^b*Division of Geological & Planetary Sciences, Caltech, Pasadena, CA 91125, USA*

Abstract

Records of relative paleointensity are subject to several sources of error. Temporal averaging due to gradual acquisition of magnetization removes high-frequency fluctuations, whereas random errors introduce fluctuations at high frequency. Both sources of error limit our ability to construct stochastic models from paleomagnetic observations. We partially circumvent these difficulties by recognizing that the largest effects occur at high frequency. To illustrate we construct a stochastic model from two recent inversions of paleomagnetic observations for the axial dipole moment. An estimate of the noise term in the stochastic model is recovered from a high-resolution inversion (CALS10k.2), while the drift term is estimated from the low-frequency part of the power spectrum for a long, but lower-resolution inversion (PADM2M). Realizations of the resulting stochastic model yield a composite, broadband power spectrum that agrees well with the spectra from both PADM2M and CALS10k.2. A simple generalization of the stochastic model permits predictions for the mean rate of magnetic reversals. We show that the reversal rate depends on the time-averaged dipole moment, the variance of the dipole moment and a slow timescale that characterizes the adjustment of the dipole

toward the time-averaged value. Predictions of the stochastic model give a mean rate of 4.2 Myr^{-1} , which is in good agreement with observations from marine magnetic anomalies.

Keywords: geodynamo, geomagnetic spectrum, stochastic model

1. Introduction

The spectrum of fluctuations in the geomagnetic dipole offers insights into the origin of the magnetic field and the dynamics of Earth's core (Constable and Johnson, 2005). Each distinct timescale bears the fingerprints of the underlying physical processes (e.g. Sakuraba and Hamano, 2007). Paleomagnetic observations are essential for characterizing the long-term behavior, yet no single source of information is sufficient to capture the full range of dynamics. Instead, we require an integrated approach to combine different types of measurements into a composite record that spans a broad range of timescales.

One important source of information comes from measurements of relative paleointensity in marine sediments (Valet, 2003). Records are stacked and calibrated using independent estimates of absolute paleointensity to produce models for the virtual axial dipole moment (VADM) over the past two million years (Valet et al., 2005; Ziegler et al., 2011). Sediments acquire a magnetization over several thousand years (Roberts and Winkholfer, 2004), so the true signal is averaged in time. Uncertainties in dating can have a similar affect because paleomagnetic records from different times may be stacked together.

Higher resolution records have been obtained for the past 10 kyr using

21 a combination of archeomagnetic and lake sediment data. These data have
22 improved spatial resolution, so the geomagnetic field can be expanded in low-
23 degree spherical harmonics (e.g. Korte and Constable, 2011). Even higher
24 resolution records are available from historical observations (Jackson et al.,
25 2000). Taken together these records provide a comprehensive description of
26 fluctuations in the dipole field, but the task of combining these results into
27 a single coherent model is a challenge.

28 Stochastic models are a useful tool because they enable quantitative pre-
29 dictions over a range of timescales. This facility is important for combining
30 different types of data with different levels of temporal resolution. There is
31 also good reason to think that stochastic models can represent the relevant
32 processes in the core. Stochastic models have been constructed from geody-
33 namo simulations with only a few model parameters, yet these models are
34 capable of reproducing most of the variability in these simulations (Kuipers
35 et al., 2009; Buffett et al., 2014; Bouligand et al., 2016).

36 Synthetic studies using geodynamo simulations are an ideal test of the
37 general approach because the simulations have relatively low numerical error
38 and we can control the temporal resolution of the output. None of these ad-
39 vantages apply when we use paleomagnetic observations to construct stochas-
40 tic models. Significant errors are present in the estimates of the dipole field,
41 which affect the construction of the stochastic model. We also need to deal
42 with temporal averaging because it limits our ability to sample the stochas-
43 tic process. The goal of this study is to address the practical limitations of
44 dealing with paleomagnetic observations and to devise a strategy for con-
45 structing models that can explain both paleomagnetic and historical records.

46 We focus primarily on the power spectrum of dipole fluctuations, although
47 we find that the resulting stochastic models can also account for the observed
48 reversal rate and the duration of polarity transitions.

49 2. Stochastic Description of Dipole Fluctuations

50 Stochastic models were introduced by Langevin (1908) to describe Brow-
51 nian motion. A small particle in water was assumed to move under the
52 combined influence of viscous resistance and a random force due to collision
53 with (unseen) water molecules. The viscous force was treated as a slowly
54 varying deterministic quantity, whereas the force due to collisions with water
55 molecules was treated as a rapidly fluctuating random process.

56 Brownian motion serves as a loose analogy for the evolution of the geo-
57 magnetic dipole moment. The deterministic part of the dipole moment rep-
58 resents the opposing influences of dipole decay and the time-averaged dipole
59 generation. Rapid fluctuations in dipole generation about the time average
60 can be attributed to (unseen) turbulent flow, which we treat as a random
61 process. We denote the axial dipole moment by $x(t)$ and describe its time
62 evolution using a stochastic differential equation (Van Kampen, 1992)

$$\frac{dx}{dt} = v(x) + \sqrt{D(x)}\Gamma(t), \quad (1)$$

63 where the drift term, $v(x)$, describes the deterministic part of the evolution
64 and the noise term, $D(x)$, defines the amplitude of the random part. The
65 time dependence of the random process, $\Gamma(t)$, is assumed to be Gaussian
66 with a vanishing time average

$$\langle \Gamma(t) \rangle = 0. \quad (2)$$

We also assume that the correlation time of the noise source is short compared with the sampling of $x(t)$. In this case the autocovariance function of $\Gamma(t)$ can be approximated by a Dirac delta function,

$$\langle \Gamma(t_1)\Gamma(t_2) \rangle = 2\delta(t_1 - t_2), \quad (3)$$

where the factor of two is a common convention (e.g. Risken, 1989).

Estimates for $v(x)$ and $D(x)$ can be extracted from a realization of the stochastic process (e.g. Friedrich et al., 2011). The drift term is defined by

$$\langle x(t + \Delta t) - x(t) \rangle = v(x)\Delta t + O(\Delta t^2) \quad (4)$$

and the noise term can be approximated by

$$\langle [x(t + \Delta t) - x(t)]^2 \rangle = 2D(x)\Delta t + O(\Delta t^2), \quad (5)$$

where the time averages are taken for a specific value of $x = x(t)$. In practice, the dipole moment is divided into a finite number of bins and a time average is evaluated for each bin. The time increment, Δt , is chosen to be long enough that $\Gamma(t)$ and $\Gamma(t + \Delta t)$ are uncorrelated, but short enough that higher order terms in Δt are small enough to neglect.

Applying (4) and (5) to the output of a geodynamo model (Buffett et al., 2014; Meduri and Wicht, 2016) shows that the drift term, $v(x)$, is well represented by

$$v(x) = -\gamma(x - \langle x \rangle), \quad (6)$$

where $\langle x \rangle$ denotes the time average and γ is a constant that defines the inverse timescale for slow adjustments of the dipole. A similar representation for $v(x)$ has been recovered from VADM estimates (Brendel et al., 2007; Buffett et al., 2013). Very similar values for the constant, $\gamma \approx 0.034 \text{ kyr}^{-1}$, were

86 reported for the SINT-2000 model of Valet et al. (2005) and the PADM2M
87 model of Ziegler et al. (2011). By comparison, the noise term, $D(x)$, has a
88 weaker dependence on x . It suffices for our purposes to treat D as a constant
89 and denote its value by D_{eq} .

90 Simple representations for the drift and noise terms permit closed-form
91 solutions for the power spectrum of fluctuations about the time average (e.g.
92 $\epsilon(t) = x(t) - \langle x \rangle$). Defining the Fourier transform of $\epsilon(t)$ by

$$\epsilon(f) = \int_{-\infty}^{\infty} \epsilon(t) e^{-i2\pi ft} dt, \quad (7)$$

93 the power spectrum becomes (Buffett and Matsui, 2015)

$$S_{\epsilon}(f) = \frac{D_{eq}}{(\gamma^2 + 4\pi^2 f^2)} S_R(f), \quad (8)$$

94 where the power spectrum for a white noise source (with a variance of 2) is

$$S_R(f) = 2. \quad (9)$$

95 The theoretical spectrum in (8) agrees well with a direct calculation of
96 the power spectrum from a geodynamo model (see Fig. 1). Departures at
97 high frequency can be improved by allowing for the influence of correlated
98 noise (Buffett and Matsui, 2015; Bouligand et al., 2016). The spectrum
99 for $\epsilon(t)$ with correlated noise (denoted by $S_{\epsilon}^c(f)$) reduces the power at high
100 frequencies, but it does not change the behavior at low frequencies. It is
101 important to note that the drift and noise terms are recovered from the
102 geodynamo model using (4) and (5) with a time difference of $\Delta t = 1$ kyr.
103 No long-period information goes into the estimation of $v(x)$ and $D(x)$, yet
104 the resulting predictions are in good agreement with the low-frequency part
105 of the spectrum. This result suggests that a simple stochastic model offers a
106 good description of long-period dipole fluctuations.

107 3. Recovering the Drift and Noise from Paleomagnetic Models

108 Several complications arise when the drift and noise terms are computed
 109 from paleomagnetic models of the dipole moment. One complication is due to
 110 random error and the other is due to temporal averaging of the fluctuations.
 111 We explore both of these complications before proposing a possible solution.

112 3.1. Influence of Random Error

113 Random error alters the estimates of the dipole moment, so the drift and
 114 noise terms are computed from

$$y(t) = x(t) + \eta(t) \quad (10)$$

115 which includes a time-dependent error $\eta(t)$. The drift term becomes

$$v(y) = \frac{\langle y(t + \Delta t) - y(t) \rangle}{\Delta t} \quad (11)$$

116 OR

$$v(y) = v(x) + \frac{\langle \eta(t + \Delta t) - \eta(t) \rangle}{\Delta t} \quad (12)$$

117 on substituting for $y(t)$ from (10). The presence of random error alters $v(y)$
 118 but the time average of the error in (12) is expected to vanish. The same is
 119 not true for the noise term. Using $y(t)$ to evaluate $D(y)$ gives

$$D(y) = \frac{\langle [y(t + \Delta t) - y(t)]^2 \rangle}{2\Delta t} \quad (13)$$

120 which can be rearranged into the form

$$D(y) = D(x) + \frac{\langle \Delta x \Delta \eta \rangle}{\Delta t} + \frac{\langle \Delta \eta^2 \rangle}{2\Delta t} \quad (14)$$

on introducing $\Delta x = x(t + \Delta t) - x(t)$ and $\Delta \eta = \eta(t + \Delta t) - \eta(t)$. Even when Δx and $\Delta \eta$ are uncorrelated, and $\eta(t)$ represents the effects of white noise, we are left with (Hoze and Holeman, 2015)

$$D(y) = D(x) + \frac{\sigma_\eta^2}{\Delta t} \quad (15)$$

where σ_η^2 is the variance of the error. Thus the influence of random error becomes acute when Δt is small. On the other hand, larger Δt causes the higher order terms in (4) and (5) to become more important.

We illustrate the problem using a synthetic example. Consider a stochastic model with a linear drift term ($\gamma = 0.034 \text{ kyr}^{-1}$) and a constant noise term ($D_{eq} = 0.069 \times 10^{44} \text{ A}^2 \text{ m}^4 \text{ kyr}^{-1}$). These numerical values were recovered by Buffett et al. (2013) from model PADM2M of Ziegler et al. (2011). A numerical realization of the stochastic model is run for 2 Myr with values of $x(t)$ recorded at 1 kyr intervals. Next we add uncorrelated and normally distributed random error to produce a noisy record, $y(t)$, where the standard deviation of the error is $\sigma_\eta = 0.5 \times 10^{22} \text{ A m}^2$. Finally, we recover a constant value for both $D(x)$ and $D(y)$ from $x(t)$ and $y(t)$; we denote these constants by D_{eq}^x and D_{eq}^y to explicitly identify the input time series.

Figure 2 shows the estimates for D_{eq}^x and D_{eq}^y as a function of Δt . At the shortest time difference, $\Delta t = 1 \text{ kyr}$, we obtain $D_{eq}^x = 0.068 \pm 0.002 \times 10^{44} \text{ A}^2 \text{ m}^4 \text{ kyr}^{-1}$ and $D_{eq}^y = 0.297 \pm 0.010 \times 10^{44} \text{ A}^2 \text{ m}^4 \text{ kyr}^{-1}$, where the uncertainties represent one standard deviation. These results are consistent with expectations from (15). Large deviations from the true value of D_{eq} are found with the noisy record when Δt is small. Smaller deviations occur as Δt increases, although these errors remain relatively large. On the other hand, the value recovered from the error-free record, $x(t)$, is reliable at small Δt but

slowly departs from the known value as Δt becomes larger. Consequently, we cannot deal with the influence of random error by arbitrarily increasing Δt .

3.2. Influence of Temporal Averaging

Temporal averaging of the paleomagnetic record can arise in several ways. Errors in dating allows measurements at different times to be stacked. In addition, magnetization is acquired in sediments over several thousand years (Roberts and Winkholfer, 2004). A prolonged acquisition time removes high-frequency variations and affects our ability to sample the stochastic process at short Δt . One way to deal with the problem of averaging is to treat the measured record as a filtered version of the true signal (e.g. Leonard, 1974). We define the measured signal, $\bar{x}(t)$, as

$$\bar{x}(t) = \int_{-\infty}^{\infty} x(t')g(t-t')dt \quad (16)$$

where the filter function, $g(t)$, smooths the true signal, $x(t)$, over some prescribed averaging time (denoted by T). Two popular filter functions are the box-car and gaussian filters (see Fig. 3). The true signal is convolved with a suitable filter function to produce the measured record.

The paleomagnetic record, $\bar{x}(t)$, still obeys a stochastic differential equation, but it is not the same as the differential equation in (1). Applying the filter to (1) gives

$$\frac{d\bar{x}}{dt} = -\gamma(\bar{x} - \langle x \rangle) + \sqrt{D_{eq}}\bar{\Gamma}(t) \quad (17)$$

where we have adopted a constant noise term and a linear drift term. The only difference in (17) is that the random process is driven by $\bar{\Gamma}(t)$ rather

166 than $\Gamma(t)$. A power spectrum for $\bar{\epsilon} = \bar{x} - \langle x \rangle$ is defined by taking the
167 Fourier transform of (17). Solving for $\bar{\epsilon}(f)$ gives

$$\bar{\epsilon}(f) = \frac{\sqrt{D_{eq}} \bar{\Gamma}(f)}{(\gamma + 2\pi i f)} \quad (18)$$

168 and the power spectrum becomes (Rice, 1954)

$$S_{\bar{\epsilon}}(f) = \frac{D_{eq}}{(\gamma^2 + 4\pi^2 f^2)} S_{\bar{\Gamma}}(f) \quad (19)$$

169 where

$$S_{\bar{\Gamma}}(f) = 2 g(f) g(f)^* \quad (20)$$

170 and $g(f)$ is the Fourier transform of the filter function. Equation (20) follows
171 from the convolution theorem (e.g. Bracewell, 1999) because convolution in
172 the time domain

$$\bar{\Gamma}(t) = \int_{-\infty}^{\infty} \Gamma(t') g(t - t') dt \quad (21)$$

173 corresponds to multiplication in the frequency domain

$$\bar{\Gamma}(f) = \Gamma(f) g(f). \quad (22)$$

174 Power spectra for $x(t)$ and $\bar{x}(t)$ are the same at low frequencies because
175 $g(f) \rightarrow 1$ as $f \rightarrow 0$ (see Fig 3).

176 We illustrate the consequences of time averaging using the stochastic
177 model from Section 3.1. A 2-Myr realization is sampled at 1-kyr intervals and
178 a smoothed version is produced using a box-car filter with an averaging time
179 of $T = 3$ kyr. Figure 4 shows the power spectrum of the filtered signal, $\bar{x}(t)$,
180 compared with the theoretical spectrum from (19). We also show the power
181 spectrum for the original (unfiltered) time series, $x(t)$, versus the theoretical
182 spectrum from (8). Both theoretical spectra are in good agreement with the

183 direct calculations from $x(t)$ and $\bar{x}(t)$. Undulations in the spectrum of $\bar{x}(t)$ is
 184 a consequence of the box-car filter, which is oscillatory in the Fourier domain.
 185 The main conclusion from this example is that temporal averaging affects
 186 only the high-frequency behavior of the record. The filtered dipole moment
 187 still obeys a stochastic differential equation and the spectrum is still reliably
 188 predicted at low frequencies from the drift and noise terms. Conversely, the
 189 low-frequency part of the spectrum constrains the drift and noise terms of
 190 the stochastic model.

191 Figure 5 shows the noise term, D_{eq} , recovered from $x(t)$ and $\bar{x}(t)$ as a
 192 function of Δt . The most reliable estimate for D_{eq} comes from $x(t)$ at the
 193 shortest possible Δt (1 kyr in this case). Temporal filtering substantially re-
 194 duces the estimate of D_{eq} at low Δt , although the recovered value approaches
 195 a constant once Δt exceeds the filter width T . A rule of thumb based on the
 196 spectrum of the filter (say $g(f) > 0.9$) is that Δt should be roughly twice T .
 197 Sampling the process at $\Delta t = 6$ kyr gives an estimate for D_{eq} that is nearly
 198 independent of Δt . Unfortunately, this estimate is well below the known
 199 value (e.g. 0.044 versus 0.069). A similar departure in D_{eq} at $\Delta t = 6$ kyr
 200 is inferred from $x(t)$ (e.g. 0.063 versus 0.069), although the error from the
 201 unfiltered time series is much smaller.

202 The preceding results show that temporal averaging can affect the ampli-
 203 tude of the noise term, particularly when Δt is smaller than the duration of
 204 the averaging. Estimates for D_{eq} appear to approach a constant value once
 205 $\Delta t > 2T$, although this constant can be significantly less than the true value.
 206 On the other hand, random noise causes the recovered estimate of D_{eq} to ex-
 207 ceed the known value by an amount $\sigma_\eta^2/\Delta t$, where σ_η^2 is the variance of the

error. Both temporal averaging and random noise have the largest affect on the high-frequency part of the spectrum. Averaging removes power at high frequency, whereas random error introduces power across all frequencies, although it is most evident at high frequency. Consequently, the low-frequency part of the spectrum is relatively unaffected by both sources of error. We exploit this result to construct a broadband paleomagnetic power spectrum.

4. A Composite Paleomagnetic Power Spectrum

We use two sources of information to construct the paleomagnetic spectrum. Model PADM2M of Ziegler et al. (2011) gives the axial dipole moment over the past 2 Myr at intervals of 1 kyr, whereas CALS10k.2 (Constable et al., 2016) gives the axial dipole moment (and other low-degree components of the magnetic field) over the past 10 kyr at 50-year intervals. Figure 6 shows the power spectrum for each model, calculated using a multi-taper method (function `pmtm` in Matlab). We also show two theoretical spectra. One spectrum is predicted using the parameters of a simple stochastic model derived from PADM2M (Buffett et al., 2013), which gave $\gamma = 0.034 \text{ kyr}^{-1}$ and $D_{eq} = 0.069 \times 10^{44} \text{ A}^2 \text{ m}^4 \text{ kyr}^{-1}$. The second spectrum is obtained by applying a gaussian filter to the stochastic model, using an averaging time of $T = 2.4 \text{ kyr}$. The sampling used to construct the stochastic model from PADM2M was $\Delta t = 5 \text{ kyr}$, so the filter required to account for the power spectrum of PADM2M is broadly compatible with the proposed rule of thumb $\Delta t \approx 2T$.

CALS10k.2 possesses more power than PADM2M at overlapping frequencies. One interpretation is that temporal averaging has a greater influence

on PADM2M, which acts to reduce the power at high frequencies. We might remedy this problem by seeking an independent estimate for D_{eq} using the higher resolution record from CALS10k.2. Figure 7 shows the resulting estimate for D_{eq} as a function of Δt . The noise term initially increases with Δt , implying temporal averaging and/or correlated noise in the stochastic model. A simple parametric fit of the form

$$D_{eq}(\Delta t) = D_{eq}(\infty)(1 - e^{-\Delta t/T}) \quad (23)$$

gives $D_{eq}(\infty) = 0.34 \times 10^{44} \text{ A}^2 \text{ m}^4 \text{ kyr}^{-1}$ for the asymptotic value of the noise term. We fit (23) through the lower limit of the estimates in Fig. 7 to account for the possible influence of random error (which tends to increase D). A correlation time of $T = 120$ years suggests that the sampling of the stochastic process should be restricted to $\Delta t > 240$ years. (We adopt $\Delta t = 300$ years as a lower limit in our subsequent discussion.)

Even though the noise term from CALS10k.2 is more than four times larger than that from PADM2M, there are several reasons to think that the estimate from CALS10k.2 is more reliable. First, the random error in CALS10k.2 is lower than that in PADM2M (Ziegler et al., 2011). Second, the short correlation time for CALS10k.2 implies much less temporal averaging. Both of these factors should reduce the errors described in the previous section. An independent assessment of the combined influence of random error and temporal averaging for CALS10k.2 suggests that the net contribution to D_{eq} is less than 25% (see Appendix). On the other hand, CALS10k.2 is too short to reliably recover the drift term, $v(x)$, because we require sampling over a range of x . Instead, we must rely on the longer record from PADM2M to estimate the slope of the drift term.

256 Recovering a direct estimate of $v(x)$ from PADM2M using (4) is not an
 257 optimal approach. Increasing the value of D_{eq} without any change in γ
 258 predicts more power at low frequencies, which is incompatible with the low-
 259 frequency part of the PADM2M spectrum. Since we expect random error and
 260 temporal averaging to have less affect at low frequencies, we choose to alter
 261 γ to maintain agreement with PADM2M at low frequencies. In effect, we
 262 are using the low-frequency spectrum of PADM2M to estimate γ once D_{eq} is
 263 inferred from CALS10k.2. The predicted power at low frequency is D_{eq}/γ^2 ,
 264 so we take $\gamma = 0.075 \text{ kyr}^{-1}$ with $D_{eq} = 0.34 \times 10^{44} \text{ A}^2 \text{ m}^4 \text{ kyr}^{-1}$ to retain
 265 consistency with the low-frequency power in PADM2M. While the slope of
 266 the drift term is more than twice the value recovered from PAD2M using
 267 (4), it is in rough agreement with the value $\gamma = 0.07 \text{ kyr}^{-1}$ estimated for the
 268 PISO-1500 model (Channell et al., 2009). (The noise term for PISO-1500
 269 near $x = \langle x \rangle$ is $0.54 \times 10^{44} \text{ A}^2 \text{ m}^4 \text{ kyr}^{-1}$, which is somewhat higher than
 270 the value recovered from CALS10k.2. Interestingly, the preferred sampling
 271 interval for PISO-1500 is 4 to 5 kyr, which is close to the sampling interval
 272 adopted previously for PADM2M and SINT-2000 (Buffett et al., 2013). Thus
 273 the time averaging in all three VADM models is roughly the same and may
 274 reflect the gradual acquisition of magnetization in sediments).

275 Selective use PADM2M and CALS10k.2 may seem ad hoc, but the un-
 276 derlying motivation is to leverage the relative strengths of these two models.
 277 Alternative strategies are possible, such as the maximum likelihood approach
 278 of Kleinhans (2012), although we are not aware of applications where these
 279 methods have been applied to multiple data sets with different resolutions,
 280 durations and accuracies. We now test the stochastic model by assessing the

internal consistency and by making predictions for the reversal rate, which can be compared against geological observations.

Internal consistency is tested by running a series of 100 realizations of the stochastic model. The model parameters are held fixed but the initial conditions and random component differ between realizations. These realizations are run for 2 Myr and the value of the dipole moment is recorded every 300 years, corresponding to the sampling interval inferred from CALS10k.2. This choice ensures that the noise source, $\Gamma(t)$, can be approximated as uncorrelated. The origin of correlation at shorter time steps might reflect the lifetime of convective eddies in the core or possibly the time required to sweep normal and reversed patches of magnetic flux across the surface of the core (Metman et al., 2017). While we could account for correlated noise in the stochastic model (Buffett and Matsui, 2015; Bouligand et al., 2016), we avoid this complication in the realizations by choosing a sufficiently large time step.

A power spectrum is computed for each realization and the results are superimposed on the power spectra computed from PADM2M and CALS10k.2 (see Fig 8a). We also show a theoretical composite spectrum, based on the parameters of the stochastic model and now including the influences of correlated noise with a correlation time of $T = 120$ years (e.g. Buffett and Matsui, 2015). A cloud of power spectra for the realizations overlap the low-frequency part of the PADM2M power spectrum and the theoretical spectrum. Comparison of the realizations in Fig 8a with the power spectrum for CALS10k.2 is not appropriate because the CALS10k.2 spectrum is computed from a 10-kyr time series. A better comparison would rely on 10-kyr realizations (see Fig8b). A series of shorter realizations produces a cloud of power spectra that

306 overlap the computed power spectrum for CALS10k.2, suggesting that the
307 revised stochastic model is broadly consistent with the CALS10k.2 model.

308 We also test the stochastic model against historical observations (Jackson
309 et al., 2000). A steady decrease in the dipole field has lowered the dipole
310 moment by $\Delta x = 0.68 \times 10^{22}$ A m² over a 150-year interval between 1860
311 and 2010 (Gillet et al., 2013). Such a change is too large to be caused by
312 the drift term, so it must be associated with the noise term. The root-
313 mean-square (rms) variation in the dipole moment due to the noise term is
314 $\langle \Delta x^2 \rangle^{1/2} = \sqrt{2D_{eq}\Delta t}$. Using the revised estimate of D_{eq} and $\Delta t = 0.15$
315 kyr, we find $\langle \Delta x^2 \rangle^{1/2} = 0.32 \times 10^{22}$ A m². Thus the historical variation is
316 larger than the expected variation, but it is not implausible. A realization of
317 the noise process is described by (Risken, 1989)

$$\Delta x = \sqrt{2D\Delta t} w \quad (24)$$

318 where w is a random variable drawn from a standard normal distribution
319 (mean of zero and variance of 1). We require $w = 2.13$ to account for the
320 recent variation in the dipole field, which would occur about 1.7% of the
321 time. The actual probability could be somewhat lower if the noise source is
322 correlated at $\Delta t = 0.15$ kyr (a likely case given our estimate of the correla-
323 tion time from CALS10k.2). The preceding estimate would then represent
324 a modest overestimate of the probability of occurrence. By comparison, the
325 original value of $D_{eq} = 0.069 \times 10^{44}$ A² m⁴ kyr⁻¹ from PADM2M would re-
326 quire $w = 4.73$ to account for the historical variation. Such an event would
327 occur less than 0.0001% of the time, so the historical record lends support
328 to the larger value for the noise term.

329 Another useful prediction of the stochastic model is the variance of the

330 dipole moment. We obtain an expression for the variance, σ_x^2 , by integrating
331 the power spectrum over frequency

$$\sigma_x^2 = \int_{-\infty}^{\infty} S_{\epsilon}(f) df = \frac{D_{eq}}{\gamma}. \quad (25)$$

332 The revised values for $D_{eq} = 0.34 \times 10^{44} \text{ A}^2 \text{ m}^4 \text{ kyr}^{-1}$ and $\gamma = 0.075 \text{ kyr}^{-1}$ give
333 $\sigma_x = 2.13 \times 10^{22} \text{ A m}^2$. While this value exceeds the estimate $\sigma_x = 1.48 \times 10^{22}$
334 A m^2 for PADM2M (Ziegler et al., 2011), it is not too far from the estimate
335 $\sigma_x = 1.97 \times 10^{22} \text{ A m}^2$ for SINT-2000 (Valet et al., 2005) and somewhat
336 smaller than the estimate $\sigma_x = 2.68 \times 10^{22} \text{ A m}^2$ for PISO-1500 (Channell
337 et al., 2009). Thus the predicted variance lies within the range of estimates
338 from recent VADM models.

339 5. Geomagnetic Polarity Reversals

340 A more general representation of the drift term is needed to describe
341 geomagnetic polarity reversals. The linear approximation in (6) is useful
342 when x varies about $\langle x \rangle$, but its utility ceases when x approaches zero
343 during a reversal. The invariance of the magnetic induction equation to a
344 change in the sign of the magnetic field suggests that $v(x)$ is an odd function
345 of x . We expect the drift term to adjust x toward the negative value of
346 the time average once x changes sign. One simple extension of the linear
347 approximation is

$$v(x) = -\frac{\gamma x}{\langle x \rangle} (x - \langle x \rangle) \quad \text{for } x \geq 0, \quad (26)$$

348 where the expected symmetry is obtained by taking $v(-x) = -v(x)$. The
349 gradient of $v(x)$ at $x = \langle x \rangle$ is consistent with the linear approximation

in (6), but the value of the drift now vanishes at $x = 0$. It is convenient to represent the drift as the negative gradient of a potential $U(x)$. Integrating (26) for the $U(x)$ gives

$$U(x) = \frac{1}{2} \frac{\gamma x^2}{\langle x \rangle} \left[\frac{2}{3} x - \langle x \rangle \right] \quad \text{for } x \geq 0 \quad (27)$$

where the integration constant is chosen to make $U(0) = 0$. A comparison of $U(x)$ with the potential recovered from the PADM2M model of Ziegler et al. (2011) is shown in Fig. 9. The barrier at $x = 0$ is comparable for both potentials, but the amplitudes of $U(x)$ differ at large $|x|$. This is mainly a consequence of increasing γ in the revised stochastic model. A larger γ produces a narrower potential well and limits the variability of x at a fixed level of noise, consistent with the predicted standard deviation $\sigma_x = \sqrt{D_{eq}/\gamma}$. We now use the generalization of the drift in (26) to predict the rate of magnetic reversals and the duration of polarity transitions.

5.1. Rates of Reversals

Random fluctuations in x enable the dipole to jump from one potential well to the other, leading to a magnetic reversal. The average frequency of this transition can be predicted using the stochastic model. Kramers (1940) derived an approximation expression for the reversal rate, r , when the barrier $\Delta U = U(0) - U(\langle x \rangle)$ is large compared with the noise D . Kramers' formula in our notation gives

$$r = \frac{\gamma}{2\pi} e^{-\Delta U/D}. \quad (28)$$

Substituting for

$$\Delta U = \frac{1}{6} \gamma \langle x \rangle^2 \quad (29)$$

370 from (27) and using the definition of the variance from (25) gives

$$r = \frac{\gamma}{2\pi} e^{-\langle x \rangle^2 / (6\sigma_x^2)} . \quad (30)$$

371 Remarkably, the rate of reversal depends on the time average, $\langle x \rangle$, the
 372 variance, σ_x^2 , and the timescale for slow adjustments of the dipole field, γ^{-1} ;
 373 the slow timescale is thought to reflect the decay time of dipole fluctuations
 374 (e.g. Gubbins and Roberts, 1987). Geodynamo simulations suggest that the
 375 dipole fluctuations can be represented by the first few decay modes (Buffett
 376 et al., 2014). Using $\langle x \rangle = 5.3 \times 10^{22} \text{ A m}^2$, $\sigma_x = 2.13 \times 10^{22} \text{ A m}^2$
 377 and $\gamma = 0.075 \text{ kyr}^{-1}$ (75 Myr^{-1}) gives $r = 4.2$ reversals per Myr, which is
 378 comparable to the observed rate over the past 30 Myr (Lowrie and Kent,
 379 2004). By comparison, a 60-Myr realization of the stochastic process yields
 380 3.9 reversals per Myr when the realization is filtered to a resolution of 30 kyr,
 381 comparable to the resolution of marine magnetic anomalies (Gee and Kent,
 382 2015). The need to filter the realization is connected to the complexity of
 383 polarity transitions when the noise term is large. We explore this question
 384 in the next section.

385 5.2. Duration of Polarity Transitions

386 The duration of polarity transitions depends on how the transitions are
 387 defined. A definition based on magnetic intensity might depend on the time
 388 required for the dipole to recover to the long-term average after a change
 389 in sign (i.e. a recovery time). This particular definition is useful for our
 390 purposes because it can be computed from the stochastic model. We expect
 391 the drift term to be small near $x \approx 0$, so the evolution of the dipole during
 392 the transition is dominated by the noise term. A useful approximation for

the time required for the field to rise above a particular threshold, x_t , is (Buffett, 2015)

$$\tau = \frac{4x_t^2}{D(0)\pi^2} \quad (31)$$

where $D(0)$ refers to the value of the noise term at $x = 0$. The general form of (31) is characteristic of a diffusive process, which includes no contribution from the drift term. A more exact treatment of the problem accounts for the drift term as x rises toward the threshold x_t . Figure 10 shows a comparison of the approximation in (31) with the value computed from a numerical solution of the Fokker-Planck equation (e.g. Risken, 1989). Including the drift term shortens the recovery, but the difference is relatively small when we adopt the revised value for D_{eq} . This implies that the recovery of the magnetic field following a reversal is driven mainly by noise (e.g. random turbulent fluctuations in the field generation).

We can compute a recovery time from the PADM2M model by interpolating the time when x rises above the time average after a reversal. Each reversal gives a different value for τ , but the average and its standard deviation are shown in Fig. 10. The agreement with theory is surprisingly good. We also show the time required for the field to drop from the time-averaged value into a reversal (i.e. a decline time). The mean decline time from PADM2M is 41 kyr, whereas the mean recovery time is 27 kyr. This asymmetry is consistent with previous observations (Valet and Meynadier, 1993). (The decline time was incorrectly reported as the recovery time in Buffett (2015), although the main point in that study was that these short durations require a noise term in excess of $D = 0.30 \times 10^{44} \text{ A}^2 \text{ m}^4 \text{ kyr}^{-1}$).

The difference between the recovery and decline times can be attributed

417 to the role of the drift term. The recovery time is shorter than the ap-
418 proximation in (31) because the drift term drives the dipole moment toward
419 the time average, increasing the rate of adjustment after a reversal. Con-
420 versely, the dipole must work against the drift term during the decline phase.
421 The approximation in (31) lies roughly midway between the estimates from
422 PADM2M, which suggests that the drift lengthens and shortens the adjust-
423 ment by comparable amounts, relative to a purely diffusive process with no
424 drift term.

425 It is reasonable to question whether the PADM2M model can adequately
426 resolve the recovery time when the short-period behavior is not sufficient
427 to compute D_{eq} . A transition that lasts $\tau \approx 30$ kyr would correspond to
428 a frequency of $f = 1/2\tau$, assuming the transition represents half a cycle.
429 A nominal frequency of 0.017 cycles kyr^{-1} lies in the part of the spectrum
430 where PADM2M and the stochastic model are broadly consistent (see Fig.
431 8). Consequently, there is internal consistency in our argument that the
432 stochastic model is in agreement with both the transition duration and low-
433 frequency power spectrum from PADM2M. It is encouraging that the same
434 stochastic model gives a reasonable estimate for the reversal rate, particularly
435 when no information about the reversal rate is used in the construction of
436 the stochastic model.

437 The dominance of the noise term during a polarity transition has inter-
438 esting consequences for the complexity of reversals. A process that is driven
439 solely by the noise term is analogous to a random walk. The probability of
440 stepping back and forth across $x = 0$ increases with the number of steps n
441 during the transition. Dasgupta and Rubin (1998) show that the expected

number of zero-crossings is proportional to \sqrt{n} . As we decrease the step size in a numerical realization, we take a large number of steps through the transition and produce a large number of zero-crossings during a single transition. In practice the time step is limited by the correlation time of the noise source to ensure that realizations of the noise are effectively uncorrelated. Consequently, the number of steps through a transition is not arbitrarily, and a representative number is liable to produce several zero crossings.

Numerical realizations with $D(0) = 0.30 \times 10^{44} \text{ A}^2 \text{ m}^4 \text{ kyr}^{-1}$ (close to the value $D = 0.34 \times 10^{44} \text{ A}^2 \text{ m}^4 \text{ kyr}^{-1}$ proposed here) produced multiple zero-crossings in about 50% of the polarity transitions when $\Delta t = 1 \text{ kyr}$ (Buffett, 2015). The average number of zero crossings is 2.8, but this number would go up if $\Delta t = 0.3 \text{ kyr}$. We could expect $3\times$ more time steps through a transition and roughly $\sqrt{3}\times$ more zero crossings (on average), corresponding to a total of 5 changes in sign during a transition. To make meaningful comparisons with geological observations we would want to remove these short-period polarity changes by filtering the numerical realization to the resolution of the observations. In the previous section we used $T = 30 \text{ kyr}$ to compare the reversal rate with estimates from marine magnetic anomalies.

6. Conclusions

Stochastic models have been successfully tested using geodynamo simulations, but their use with paleomagnetic observations requires departures from the standard approach. Two main difficulties are identified. The first is due to random error in the estimates of the dipole moment, which cause the noise term to be over-estimated. The significance of this problem depends

on the sampling interval, Δt , and the largest affects occur at short Δt . A second difficulty arises from temporal averaging of dipole fluctuations, either due to errors in dating or gradual acquisition of magnetization in sediment. In either case, temporal averaging reduces the noise term at short Δt , although estimates for D often converge to a constant value as Δt increases. Unfortunately, the noise term does not necessarily converge to the correct value.

An important feature of both random error and temporal averaging is that the largest affects are predicted at high frequency. Because the low-frequency behavior is nearly unaltered, we can use the low-frequency part of the observed power spectrum as a constraint on the stochastic model. We illustrate the approach using the PADM2M model of Ziegler et al. (2011) and the CALS10k.2 model of Constable et al. (2016). An estimate of the noise term is recovered from the high-resolution CALS10k.2 model, while the slope of the drift term, γ , is estimated from the low-frequency part of the spectrum for PADM2M. Realizations of the stochastic model yield a composite power spectrum that agrees reasonably well with both PADM2M and CALS10k.2.

A simple generalization of the stochastic model is needed to allow large deviations from the time-averaged moment. This modification enables predictions for the mean rate of reversal. A reversal in the stochastic model occurs when a realization jumps between the minima in a double-well potential. Application of Kramers' formula (Kramers, 1940) gives a surprisingly simple expression for the reversal rate. We find that the reversal rate can be defined in terms of the time-averaged dipole moment, the variance of the dipole moment and a slow timescale that characterizes the adjustment of

the dipole toward the time-averaged value. Using values from the stochastic model gives a mean rate of 4.2 Myr^{-1} , which is in good agreement with observations (Lowrie and Kent, 2004). Comparable rates are obtained from realizations of the stochastic process, provided we filter the realization to the same resolution as the observations. The need for temporal filtering arises from the importance of noise in driving polarity transitions. Multiple polarity changes can occur within a single transition field, so a quantitative comparison with observations depends on the temporal resolution of those observations.

Acknowledgment

This work is supported by the National Science Foundation (EAR-1644644) and by a Summer Undergraduate Research Fellowship (SURF) from Caltech.

Appendix: Combined Influence of Random Error and Time Averaging

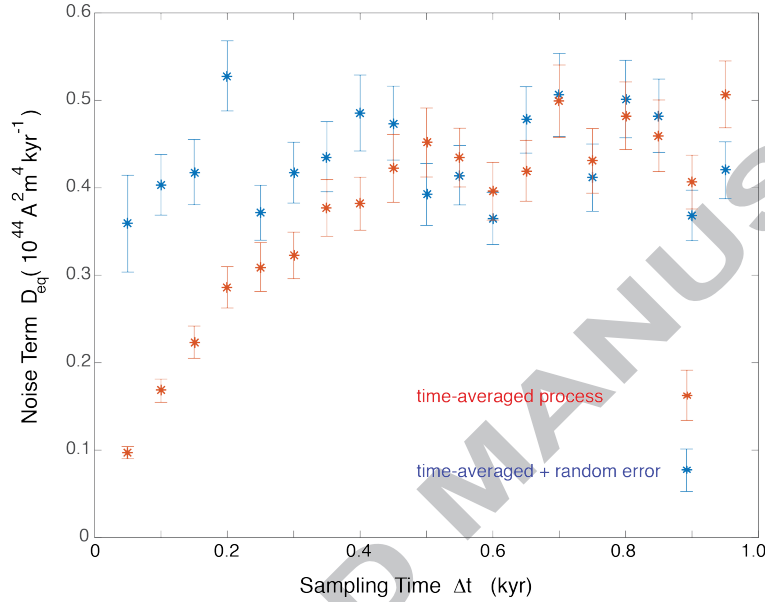
Random error and time averaging have opposite effects on estimates for the noise term in a stochastic model. Random error increases the noise term, whereas time averaging tends to reduce D_{eq} when Δt is less than roughly twice the averaging time. The combined influence of both error sources depends on their relative magnitude. As an example, we consider a realization that approximates the CALS10k.2 model. We adopt $\gamma = 0.075 \text{ kyr}^{-1}$ and $D_{eq} = 0.34 \times 10^{44} \text{ A}^2 \text{ m}^4 \text{ kyr}^{-1}$ for the parameters of the stochastic model and run a 10-kyr realization with time steps at a 50-year interval. Random error with a standard deviation of $\sigma_\eta = 0.4 \times 10^{22} \text{ A m}^2$ is added to the

realization and a box-car filter is applied with an averaging time of $T = 150$ years. All of these values are chosen to approximate the statistical properties of CALS10k.2.

Figure A1 shows the recovered estimates for D_{eq} as a function of the sampling time Δt for both the time-averaged process and the time-averaged process with random error. Estimates for D_{eq} from the time-averaged process increase with Δt and approach a constant value at large Δt . We would obtain $D_{eq} = 0.32 \times 10^{44} \text{ A}^2 \text{ m}^4 \text{ kyr}^{-1}$ for the recommended sampling interval of $\Delta t = 2T = 300$ years. Addition of random error to the process produces much higher estimates for D_{eq} at small Δt , consistent with expectations for random errors. We obtain $D_{eq} = 0.42 \times 10^{44} \text{ A}^2 \text{ m}^4 \text{ kyr}^{-1}$ at $\Delta t = 300$ years and somewhat lower values if we fit a curve through the lower limit of estimates (as done in the text). The discrepancy from the known value is about 24% or less.

The time-averaged process with random error looks qualitatively different than the estimates recovered from CALS10k.2 (see Fig. 7). In particular, the estimates from CALS10k.2 are much lower at small Δt . One interpretation is that the actual random errors in CALS10k.2 are lower than $\sigma_\eta = 0.4 \times 10^{22} \text{ A m}^2$. Alternatively, we might appeal to a longer effective time-averaging (i.e. larger T), which would lower the amplitude of the time-averaged error. On the other hand, it would be difficult to account for the observed dependence of D_{eq} on Δt in CALS10k.2 when T was much larger than 150 years. It is possible that the reported error for CALS10k.2 includes offsets or biases, which would not affect the recovered estimates for D_{eq} . Assessing the error in paleomagnetic models is a difficult challenge, and it is likely that the error

539 in CALS10k.2 is more complicated than the simple representation considered
 540 here. Still, the preceding example suggests reasonable estimates for D_{eq} can
 541 be recovered from a shorter, high-resolution model.



542

543 **Figure A1.** Recovery of noise term D_{eq} from a 10-kyr realization of the
 544 preferred stochastic model. A box-car filter is applied to the realization
 545 with and without the addition of random error. Sampling the process at
 546 $\Delta t = 2T = 300$ years gives a reasonable estimate for D_{eq} , even when a
 547 realistic level of random error is added to the process.

548 Brendel, K., Kuipers, J., Barkema, G.T., Hoyng, P., 2007. An analysis of the
 549 fluctuations of the geomagnetic dipole, *Phys. Earth Planet. Inter.*, 162,
 550 249-255.

551 Bouligand, C., Gillet, N., Jault, D., Schaeffer, N., Fournier, A. and Aubert,

- 552 J., 2016. Frequency spectrum of the geomagnetic field harmonic coefficients
553 from dynamo simulations, *Geophys. J. Int.*, 207, 1142-1157.
- 554 Bracewell, R., 1999. *The Fourier Transform and its Applications*, 3rd ed.,
555 McGraw-Hill, New York.
- 556 Buffett, B.A., Ziegler, L. and Constable, C.G., 2013. A stochastic model for
557 palaeomagnetic field variations, *Geophys. J. Int.*, 195, 86-97.
- 558 Buffett, B.A., King, E.M. and Matsui, H., 2014. A physical interpretation of
559 stochastic models for fluctuations in the Earth's dipole, *Geophys. J. Int.*,
560 199, 597-608.
- 561 Buffett, B. and Matsui, H., 2015. A power spectrum for the geomagnetic
562 dipole moment, *Earth Planet. Sci. Lett.*, 411, 20-26.
- 563 Buffett, B., 2015. Dipole fluctuations and the duration of geomagnetic po-
564 larity transitions, *Geophys. Res. Lett.*, 42, 7444-7451.
- 565 Channell, J.E.T., Xuan, C., and Hodell, D.A., 2009. Stacking paleointensity
566 and oxygen isotope data for the last 1.5 Myr (PISO-1500), *Earth Planet.*
567 *Sci. Lett.*, 283, 14-23.
- 568 Constable, C. and Johnson, C., 2005. A paleomagnetic power spectrum,
569 *Phys. Earth Planet. Inter.*, 153, 61-73.
- 570 Constable, C., Korte, M. and Panovska, S., 2016. Persistent high paleosecular
571 variation activity in southern hemisphere for at least 10,000 years, *Earth*
572 *Planet. Sci. Lett.*, 453, 78-86.

- 573 Dasgupta, A. and Rubin, H., 1998. Zero crossings of a gaussian process ob-
574 served at discrete random times and some peculiar connections to the
575 simple random walk, *Technical Report 97-23*, Department of Statistics,
576 Purdue University, West Lafayette, IN.
- 577 Friedrich, R., Peinke, J., Sahimi, M., and Reza Rahimi Tabar, M., 2011.
578 Approaching complexity by stochastic methods: From biological system
579 to turbulence, *Phys. Rep.*, *506*, 87-162.
- 580 Gee, J.S. and Kent, D.V., 2015. Sources of oceanic magnetic anomalies and
581 the geomagnetic polarity timescale, *Treatise on Geophysics*, 2nd Ed., *Vol.*
582 *5*, 419-460.
- 583 Gillet, N., Jault, D., Finlay, C. and Olsen, N., 2013. Stochastic model of the
584 Earth's magnetic field: Inversion for covariances over the observatory era,
585 *Geochem. Geophys. Geosys.*, *14*, 766-786.
- 586 Gubbins, D. and Roberts, P.H., 1987. Magnetohydrodynamics of the Earth's
587 core, in *Geomagnetism*, vol. 2, ed. Jacobs, J.A., Academic Press.
- 588 Hoze, N. and Holeman, D., 2015. Recovering a stochastic process from super-
589 resolution noisy ensembles of single particle trajectories, *Phys. Rev. E.*, *92*,
590 052109.
- 591 Jackson, A., Jonker, A.R.T., and Walker, M.R., 2000. Four centuries of ge-
592 omagnetic secular variation from historical records, *Phil. Trans. R. Soc.*
593 *Lond. A*, *358*, 957-990.
- 594 Kleinhans, D., 2012. Estimation of drift and diffusion functions from time-
595 series data: A maximum likelihood framework, *Phys. Rev. E*, *85*, 026705.

- 596 Kramers, H.A., 1940. Brownian motion in a field of force and the diffusion
597 model of chemical reactions, *Physica*, 7, 284-304.
- 598 Kuipers, J., Hoyng, P., Wicht, J. and Barkema, G.T., 2009. Analysis of the
599 variability of the axial dipole moment of a numerical geodynamo model,
600 *Phys. Earth Planet. Inter.*, 173, 228-232.
- 601 Korte, M. and Constable, C.G., 2011. Improving geomagnetic field recon-
602 structions for 0-3 ka, *Phys. Earth Planet. Inter.*, 188, 247-259.
- 603 Leonard, A., 1974. Energy cascade in large-eddy simulations of turbulent
604 flows, *Adv. Geophys.*, 18, 237-248.
- 605 Lowrie, W. and Kent, D.V., 2004. Geomagnetic polarity timescale and re-
606 versal frequency regime, in Channell, J.E.T, Kent, D.V., Lowrie, W. and
607 Meert, J., (eds.) *AGU Geophysical Monograph*, 145, Timescales of the Pale-
608 omagnetic Field, 117-129, Washington DC, American Geophysical Union.
- 609 Matsui, H., King, E. and Buffett, B., 2014. Multi-scale convection in a
610 geodynamo simulation with uniform heat flux along the outer boundary,
611 *Geochem. Geophys. Geosys.*, 15, doi: 10.1029/2014GC005432.
- 612 Meduri, D.G. and Wicht, J., 2016. A simple stochastic model for dipole
613 moment fluctuations in numerical dynamo simulations, *Front. Earth Sci.*,
614 4, doi: 10.3389/feart.2016.00038.
- 615 Metman, M.C., Livermore, P.W. and Mound, J.E., 2017. The reversed and
616 normal flux contributions to axial dipole decay for 1880-2015, *Phys. Earth
617 Planet. Inter.*, 271, xx-yy.

- 618 Langevin, P., 1908. Sur la théorie due mouvement brownien, *C. R. Acad.*
619 *Sci.*, 146, 530-533.
- 620 Olson, P., Christensen, U.R., and Driscoll, P.E., 2012. From superchrons
621 to secular variations: A broadband dynamo frequency spectrum for the
622 geomagnetic dipole, *Earth Planet. Sci. Lett.*, 319, 75-82. I
- 623 Percival, D.B. and Walden, A.T., 1993. *Spectral analysis for physical appli-*
624 *cations: multi taper and conventional univariate techniques*, Cambridge
625 University Press, Cambridge.
- 626 Rice, S.O., 1954. Mathematical analysis of random noise, in *Selected papers*
627 *on noise and stochastic processes*, ed. N. Wax, Dover, New York.
- 628 Risken, H., 1989. *The Fokker-Planck Equation*, 2nd Ed., Springer-Verlag.
- 629 Roberts, A.P. and Winkholfer, M., 2004. Why are geomagnetic excursions
630 not always recorded in sediments? Constraints from post-depositional re-
631 manent magnetization lock-in modeling, *Earth Planet. Sci. Lett.*, 227, 345-
632 359.
- 633 Sakuraba, A. and Hamano, Y., 2007. Turbulent structure in Earth's fluid
634 core inferred from time series of geomagnetic dipole moment, *Geophys.*
635 *Res. Lett.*, 34, L15308, doi: 10.1029/2007GL029898.
- 636 Valet, J.-P., Meynadier, L., 1993. Geomagnetic field intensity and reversals
637 during the past four million years, *Nature*, 366 234-238.
- 638 Valet, J.-P., 2003. Time variations in geomagnetic intensity, *Rev. Geophys.*,
639 41, 1004, doi: 10.1029/2001RG000104.

- 640 Valet, J.-P., Meynadier, L., Guyodo, Y., 2005. Geomagnetic field strength
641 and reversal rate over the past 2 million years, *Nature*, 435, 802-805.
- 642 Van Kampen, N.G., *Stochastic Methods in Physics and Chemistry*, North-
643 Holland, Amsterdam.
- 644 Ziegler, L.B., Constable, C.G., Johnson, C.L., Tauxe, L., 2011. PADM2M:
645 a penalized maximum likelihood model of the 0-2 Ma paleomagnetic axial
646 dipole moment, *Geophys. J. Int.*, 184, 1069-1089.

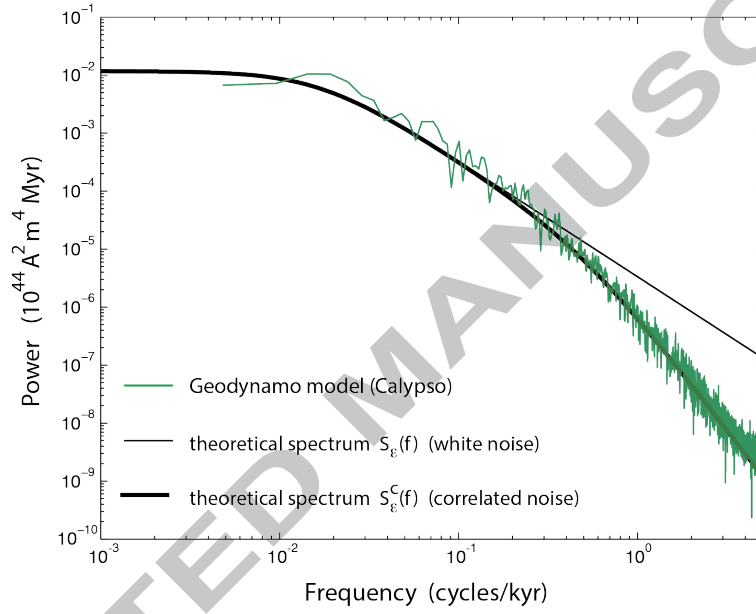


Figure 1: A power spectrum of dipole fluctuations from a numerical geodynamo simulation (Matsui et al., 2014), compared to predictions from two stochastic models. One stochastic model assumes a white noise source and the other assumes correlated noise. Both models are capable of predicting the low-frequency fluctuations even though the drift and diffusion terms are constructed from short-period information.

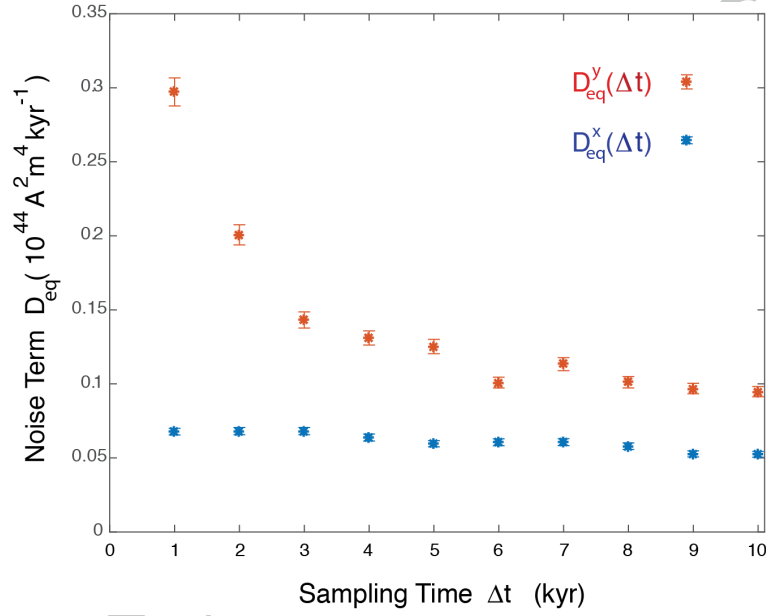


Figure 2: Estimates for the noise term, $D_{eq}(\Delta t)$, computed from exact $x(t)$ and noisy $y(t)$ time series. Addition of random error to $y(t)$ causes D_{eq}^y to depart from the known value $D_{eq} = 0.069 \times 10^{44} \text{ A}^2 \text{ m}^4 \text{ kyr}^{-1}$. Calculations using $x(t)$ reproduce the known value to within the uncertainties at $\Delta t = 1 \text{ kyr}$. Discrepancies in $D_{eq}^x(\Delta t)$ increase slowly with Δt due to unmodelled contributions from higher-order powers in Δt .

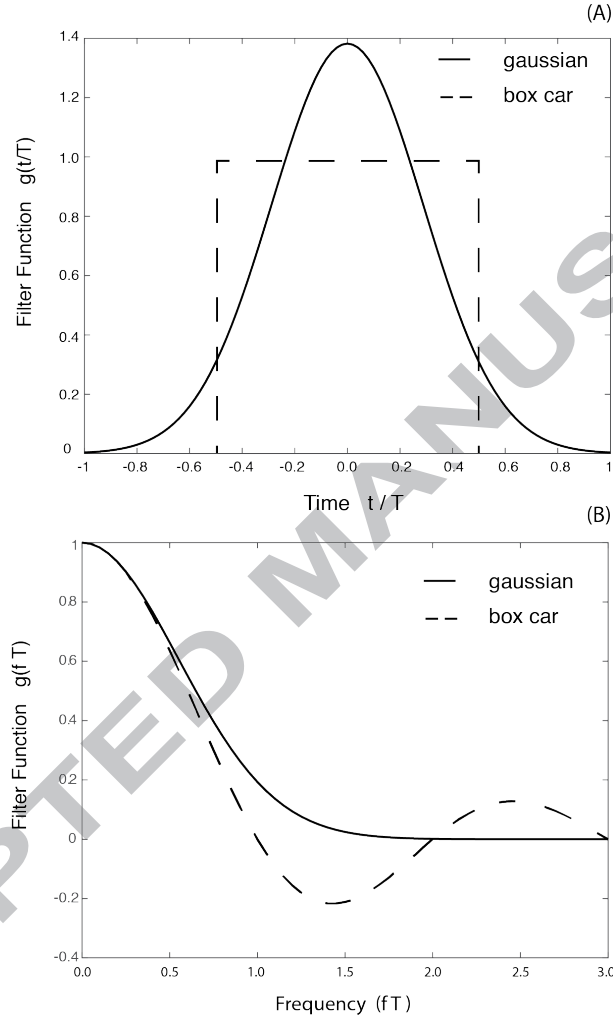


Figure 3: (A) Two commonly used filters are the Gaussian, $g(t) = (6/\pi T^2)^{1/2} \exp(-6t^2/T^2)$, and the box car, $g(t) = 1/T$ for $|t| < T/2$, where T is the averaging time. (B) Fourier transforms are given by $g(f) = \exp(-4\pi^2 f^2 T^2/24)$ and $g(f) = \sin(\pi f T)/\pi f T$, respectively.

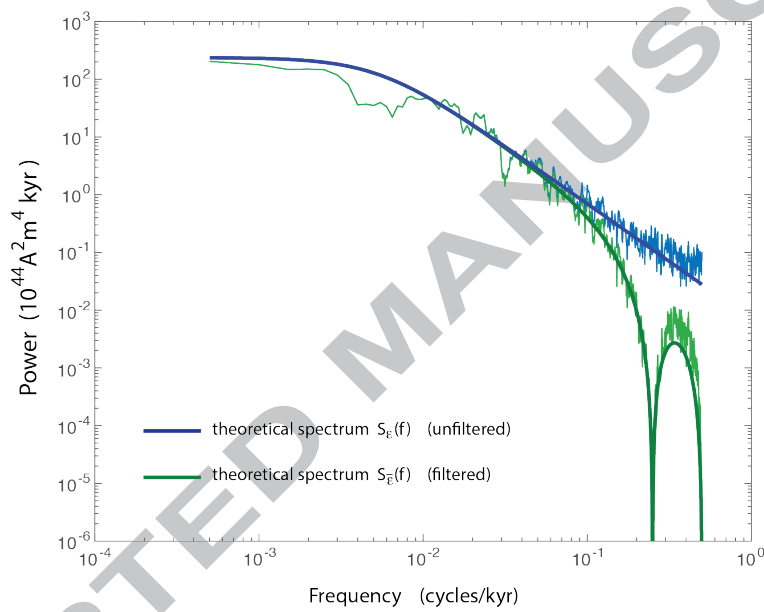


Figure 4: Power spectra of $x(t)$ (blue) and $\bar{x}(t)$ (green) compared with theoretical spectra $S_\epsilon(f)$ and $S_{\bar{\epsilon}}(f)$ (see text). Undulations in the filtered spectrum arise from the box-car filter, which is oscillatory in the frequency domain.

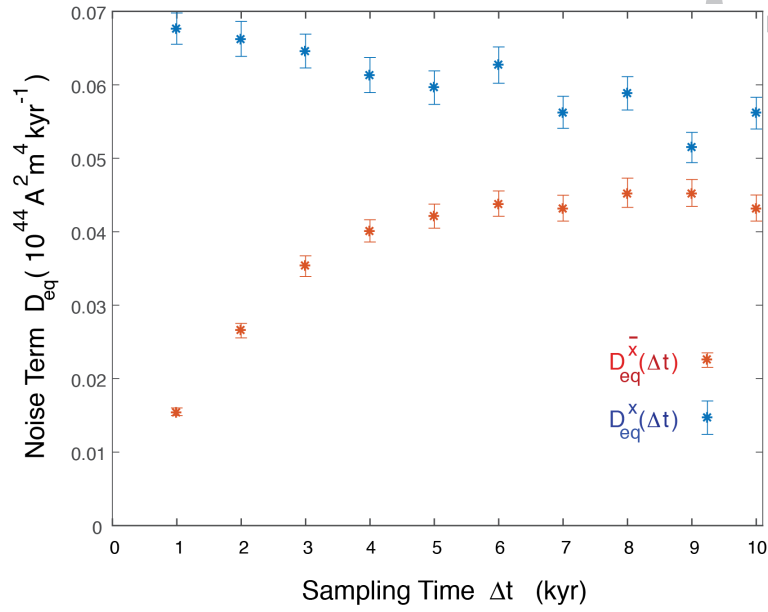


Figure 5: Estimates for the noise term, $D_{eq}(\Delta t)$, computed from exact $x(t)$ and filtered $\bar{x}(t)$ time series. Temporal averaging substantially reduces the noise term when Δt is less than the averaging time $T = 3$ kyr. Estimates for $D_{eq}^{\bar{x}}(\Delta t)$ approach a constant value once $\Delta t > 2T$.

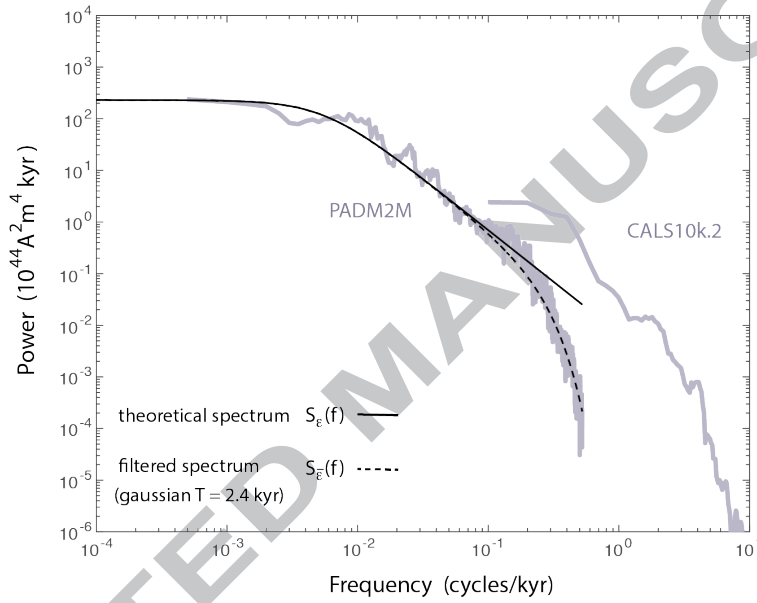


Figure 6: Power spectra computed from PADM2M and CALS10k.2 using a multi-taper method. Theoretical spectra $S_\epsilon(f)$ and $S_{\bar{\epsilon}}(f)$ are based on the stochastic model derived from PADM2M and a filtered version of the stochastic model. We apply a Gaussian filter with an averaging time of $T = 2.4 \text{ kyr}$ to account for the abrupt decrease in power of PADM2M at high frequency.

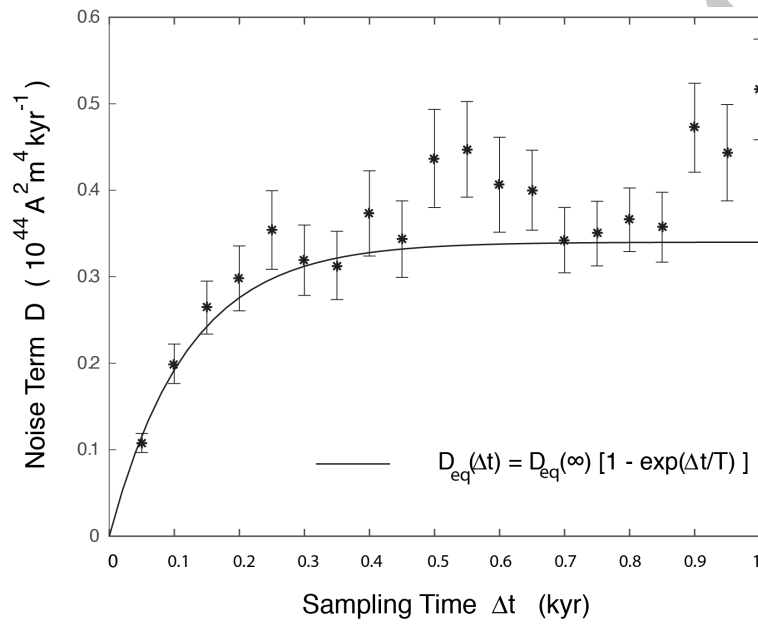


Figure 7: Estimates for the noise term, D_{eq} , recovered from CALS10k.2 as a function of sampling time Δt . A simple parametric fit to $D_{eq}(\Delta t)$ in (23) gives $D_{eq}(\infty) = 0.34 \times 10^{44} \text{ A}^2 \text{ m}^4 \text{ kyr}^{-1}$. The effective correlation time of the noise source is $T = 120$ years.

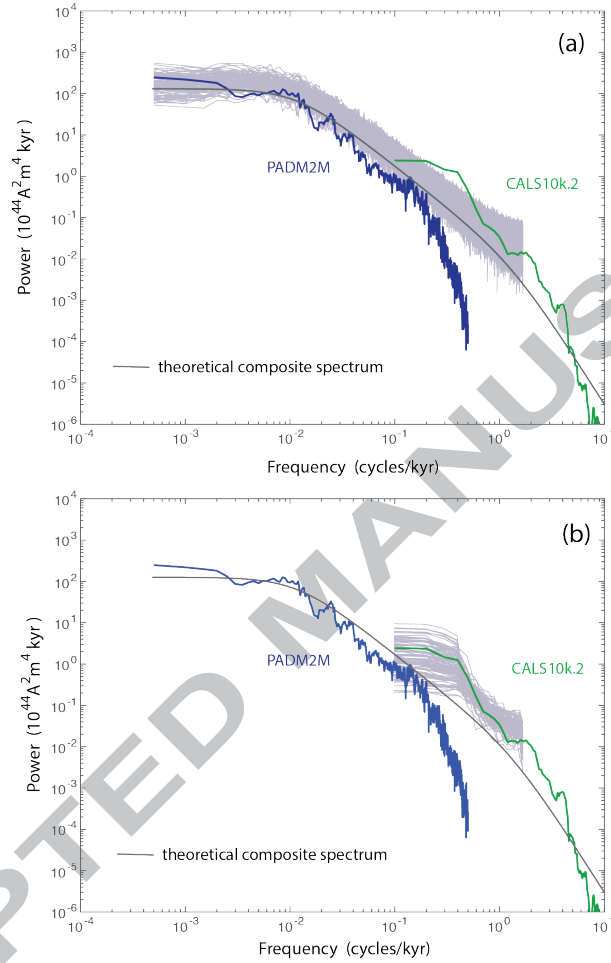


Figure 8: (A) Power spectra from 100 realizations of the stochastic model (light gray) compared with the power spectra computed from PADM2M (blue) and CALS10k.2 (green). A theoretical spectrum (dark gray) is based on the parameters of the revised stochastic model and the influences of correlated noise with a correlation time of $T = 120$ years. The ensemble of realizations is compatible with PADM2M at low frequencies. (B) Power spectra of 100 shorter (10-kyr) realizations of the stochastic model agree well with the power spectrum for CALS10k.2.

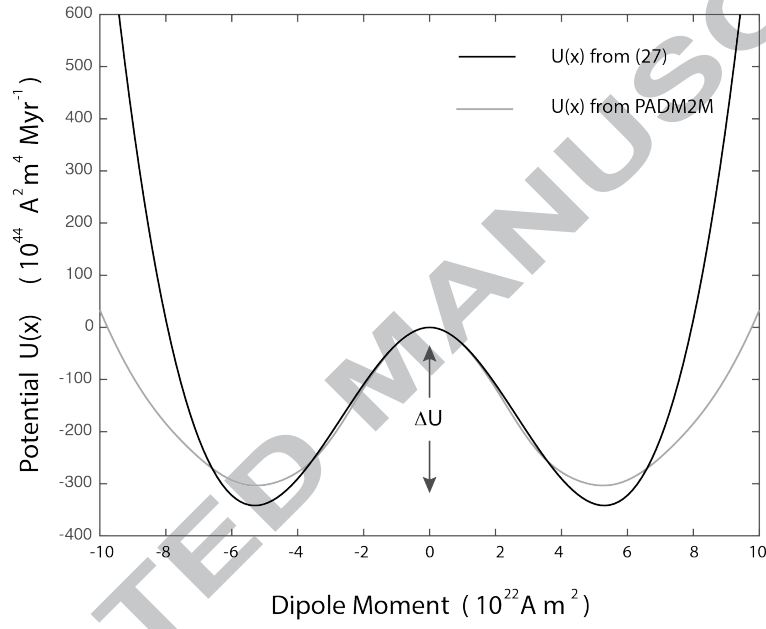


Figure 9: Potential $U(x)$ computed from (27) compared with a potential recovered from PADM2M. Both potentials have comparable barriers, ΔU , but different amplitudes at large $|x|$. The width of the potential well is defined by the second derivative $U''(x) = -\gamma$ at $x = \pm \langle x \rangle$. We use $\gamma = 0.075 \text{ kyr}^{-1}$ for the potential in (27).

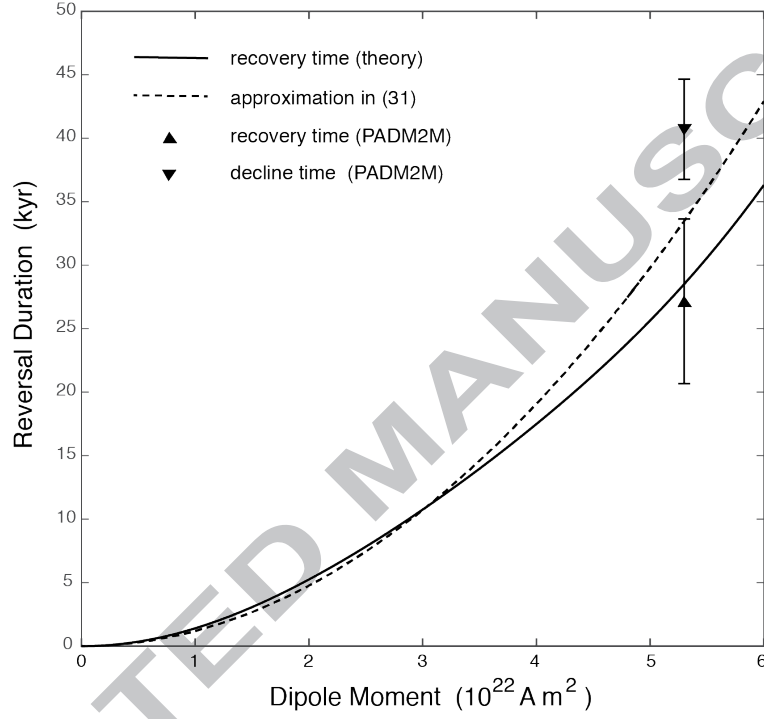


Figure 10: Mean recovery time for the dipole moment following a reversal. A numerical solution of the Fokker-Planck equation (theory) is compared with the approximation in (31), where the drift term is assumed to vanish. Discrete estimates from PADM2M are shown for the recovery and decline times. The recovery time agrees well with the theoretical estimate for recovery, whereas the decline time exceeds the recovery time due to contributions from the drift term.

Characterize the influence of random error and temporal averaging in paleomagnetic observations

Construct stochastic model using two compilations of paleomagnetic observations

Predict a composite, broadband power spectrum for dipole fluctuations

Stochastic model provides a quantitative estimate for reversal rate